

Nanocomposites based on water soluble polymers and unmodified smectite clays

K E STRAWHECKER, Veeco Instruments Inc, USA and
E MANIAS, The Pennsylvania State University, USA

8.1 Introduction

Polymer/layered-silicate hybrids – nanocomposites – have attracted strong interest in today's materials research, as it is possible to achieve impressive enhancements of material properties compared to the pure polymers. Especially when these properties depend on the surface area of the filler particles, small amounts (typically less than 5%) of nm-thin layered inorganic fillers give rise to the same level of mechanical and thermal improvements as are typically achieved with loadings of 30–50% of micron-sized fillers. Examples of such materials enhancements are decreased permeability to gases and liquids, better resistance to solvents, increased thermal stability, and improved mechanical properties. Nanometer-thin layered materials used to form polymer nanocomposites include montmorillonite clays, synthetic 2:1 aluminosilicates, metal phosphates, transition metal chalcogenides, and complex oxides, to name a few.^{1–6} In some cases, properties are observed in nanoscale materials that have not been realized in more conventional material structures, as for example flame retardant character.⁷ Since this occurs without sacrificing properties such as optical clarity they are good choices as fillers in applications such as coatings and packaging.

Sodium montmorillonite (MMT) is a naturally occurring 2:1 phyllo-silicate, capable of forming stable suspensions in water. This hydrophilic character of MMT also promotes dispersion of these inorganic crystalline layers in water soluble polymers such as poly(vinyl alcohol)⁸ and poly(ethylene oxide).^{9,10} Inspired from those studies, this work is focused on investigating the properties of poly(vinyl alcohol)/MMT nanocomposite hybrids. Poly(vinyl alcohol) (PVA) is a water soluble polymer extensively used in paper coating, textile sizing, and flexible water soluble packaging films.¹¹ These same applications stimulate an interest in improving mechanical, thermal, and permeability properties of thin nanocomposite films, ultimately with the hope of retaining the optical clarity of PVA. PVA/layered silicate nanocomposite materials may offer a viable alternative for these applications to heat treatments (that may

cause polymer degradation) or conventionally filled PVA materials (that are optically opaque).

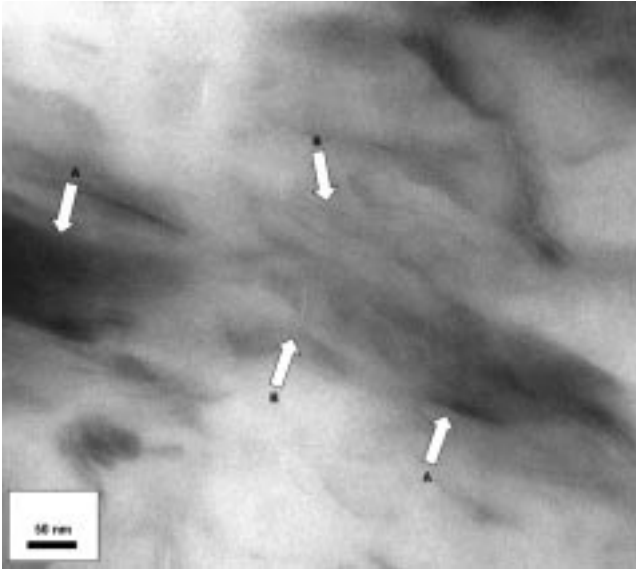
Polymer crystallization behavior near an inorganic surface has been the focus of extensive study.¹² In most cases the inorganic surface is shown to produce a nucleating or epitaxial effect,^{2,13–15} which often stabilizes the bulk crystal phase or, in some cases, promotes growth of a different crystal phase. The polymer mechanical and thermal properties can be enhanced through this mechanism, where the surface-nucleated crystalline phase has better mechanical and thermal characteristics than the bulk crystal phases.^{2,14–15,17} Fillers with large surface area maximize these filler-induced enhancements of the material properties; a dramatic manifestation of such a response is found in nylon-6/montmorillonite nanocomposites.^{2,14,15} Less dramatic property enhancements are found in systems where the bulk crystalline phase is simply stabilized via the incorporation of heterogeneous nucleation sites, such as in polypropylene/organo-montmorillonite systems.¹⁸

The nylon-6/inorganic hybrids show dramatic enhancements in their mechanical and thermal properties upon addition of a minute amount (2–10 wt.%) of montmorillonite (MMT),² a nanometer thin mica-type layered silicate with a surface area of about 750 m²/g. This was later attributed to a filler-stabilized γ crystalline phase of nylon-6 formed at the silicate surface.^{14,15,19} PVA/layered-silicate nanocomposites also possess such filler-induced property enhancements,¹⁶ which were also attributed to the existence of a non-bulk-like crystalline structure promoted when Na⁺ montmorillonite (MMT) is added to PVA.¹⁷

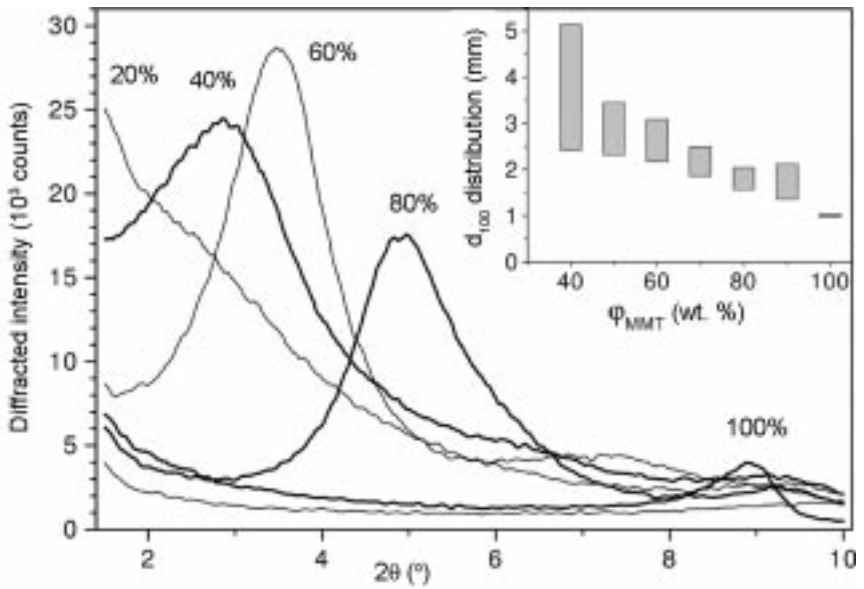
8.2 Dispersion of Na⁺ montmorillonite in water soluble polymers

Bright field TEM is used to directly view the hybrid structure for the nanocomposites formed, with the emphasis on the dispersion of the nanometer thin layered fillers in the polymer matrix. A typical TEM image is shown in Fig. 8.1 for the 20 wt.% MMT nanocomposite. Extensive TEM observations reveal a coexistence of silicate layers in the intercalated (label 'A') and the exfoliated ('B') states. We refer to intercalated layers/structures where the inorganic layers maintain the parallel registry of pristine silicates, and are separated by ultra-thin (1.3–5 nm) PVA films. Due to the periodic parallel assembly of the silicates, the intercalated structures give rise to X-ray diffraction peaks. We refer to exfoliated layers/structures where the layers are much further apart ($\gg 5$ nm), and in general both the layer registry and the parallel stacking are lost.

The periodic intercalated structure can be quantified through powder XRD. Comparison of the intercalated gallery height with that of the pristine MMT (9.7 Å) measures the thickness of the PVA/Na⁺ film. Fig. 8.2 shows XRD scans for concentrations of 20, 40, 60, 80 and 100 wt.% MMT; the inset shows the corresponding d-spacing distributions for the same concentrations. The



8.1 TEM image of 20 wt.% MMT/PVA nanocomposite revealing the coexistence of intercalated (A) and exfoliated (B) MMT layers. Copyright © *Chem. Mater.* 2000, vol. 12, pp. 2943–2949.



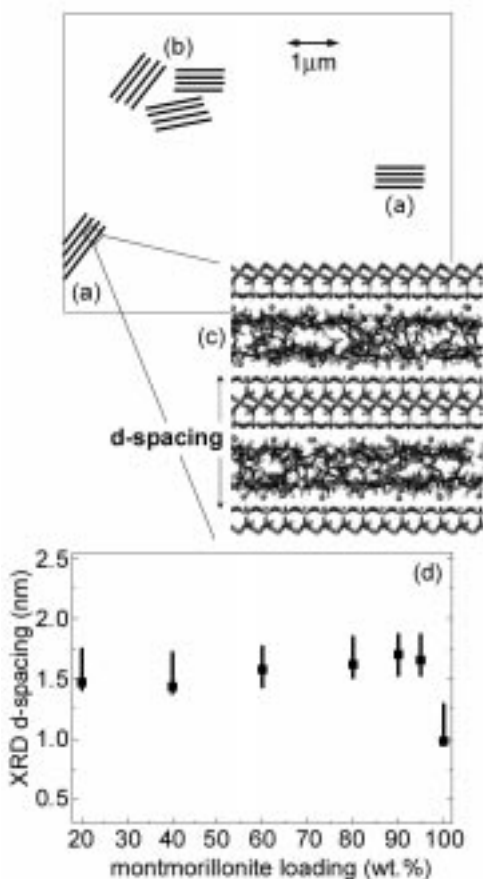
8.2 X-ray diffraction of the PVA/MMT hybrids as a function of ϕ_{MMT} . The inset shows the distribution of the MMT intercalated d-spacings for the respective hybrids. Copyright © *Chem. Mater.* 2000, vol. 12, pp. 2943–2949.

distribution of the intercalated d-spacings is calculated at half maximum of the d_{001} peak and the range of observed periodicities is given by bars (Fig. 8.2, inset) for each sample. Both the d-spacings, as well as their distributions, decrease systematically with higher silicate loadings, from 40 to 90 wt.% MMT. For lower inorganic filler concentrations, the XRD diffraction peak that corresponds to the silicate gallery d-spacing moves below $2\theta = 1.5^\circ$. This suggests that, if there still exist periodic assemblies of intercalated MMT layers, these are characterized by d-spacings larger than 5 nm. In addition, for all the nanocomposite XRDs, the background is higher than expected for simple mixtures of PVA and MMT, suggesting the existence of exfoliated inorganic layers throughout the polymer matrix. Thus, both XRD and TEM consistently show that these samples are in a hybrid structure where both intercalated and exfoliated silicate layers coexist in considerable ratios.

At first glance, this dependence of the intercalated structure and d-spacing on the polymer/silicate mass ratio seems to be at odds with the theoretical expectations.^{20,21} The equilibrium hybrid structure predicted from the thermodynamics corresponds to an intercalated periodic nanocomposite (with a d-spacing around 1.8 nm) which is expected to be independent of the polymer/silicate composition.²⁰ However, thermodynamics can only predict the *equilibrium* structure. In our case though, the hybrid structure that we find is actually kinetically dictated: In the water solution of poly(vinyl alcohol) and montmorillonite the layers remain in colloidal suspension. Where this suspension is slowly dried, the silicate layers remain distributed and embedded in the polymer gel. With further drying, to remove all water, although thermodynamics would predict the MMT layers to reaggregate in an intercalated fashion, the slow polymer dynamics trap some of the layers apart, and therefore remain dispersed in the polymer. Obviously, these kinetic constraints by the polymer become less important as the polymer-to-silicate fraction decreases, and consequently, for higher ϕ_{MMT} , intercalated structures are formed. For these periodic structures, the variation of the d-spacing with ϕ_{MMT} reflects the different polymer/silicate weight ratios, and with increasing ϕ_{MMT} the intercalated d-spacing converges to the equilibrium 1.8 nm.

Dispersion of silicates in water soluble polymers need not result in kinetically trapped systems, and such is the behavior of PEO/ Na^+ MMT hybrids. The structure of these polymer/inorganic hybrids is well known (Fig. 8.3), studied extensively both experimentally,^{9,10,22} as well as by molecular simulations,^{23,24} and is markedly independent of the filler loading. When enough PEO exists in the composite an intercalated structure is formed (with d-spacings distributed around 1.7 nm, which corresponds to a PEO bilayer of about 0.8 nm thickness). For composites with extremely small amounts of PEO ('polymer-starved' composites at montmorillonite loadings of $\phi_{\text{MMT}} > 90\%$), an intercalated monolayer of PEO can also be observed, with an intercalated d-spacing of about 1.37 nm. These latter structures are of no interest to this present work. For the

montmorillonite loadings of interest here ($\phi_{\text{MMT}} = 1\text{--}10\text{ wt.}\%$) the layered silicates retain their pristine parallel registry, but there is an increase in the d-spacing (Fig. 8.3(d)) due to the intercalation of PEO in the interlayer gallery (Fig. 8.3(c)). Successive single layers self-assemble in stacks (tactoids, Fig. 8.3(a)), in a highly parallel stacking that can give rise to $00l$ XRD diffraction peaks up to the 11th order.⁹ These micron size tactoids are dispersed in the PEO matrix – either isolated or in groups of tactoids (agglomerates, Fig. 8.3(b)) – separated by regions of pure polymer (Fig. 8.3).



8.3 Schematic of the PEO/ Na^+ MMT intercalated nanocomposites. The layered inorganic MMT layers assemble in a parallel fashion, creating stacks of layers referred to as tactoids (a), and most times tactoids are found in groups referred to as agglomerates (b), separated by bulk-like polymer regions. Within the tactoid, MMT layers are separated by a 0.8 nm film of PEO (c), which is stable through a wide range of MMT loadings as seen in the X-ray diffraction data (d). The MMT layers bear a large number of Na^+ (one cation per 70 \AA^2), depicted by dots in (c). Copyright © *Chem. Mater.* 2003, vol. 15, pp. 844–849.

8.3 Crystallization behavior

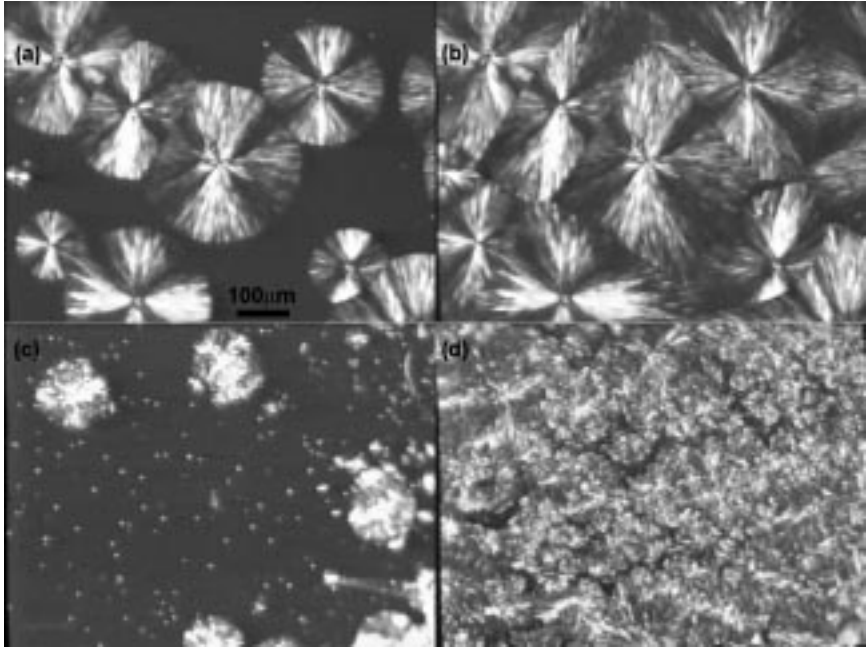
Methods used to compare and contrast the crystallization behavior of water soluble crystalline polymers with dispersed silicates may include cross-polarization optical microscopy (CPOM) or atomic force microscopy (AFM), depending upon physical properties of the materials such as spherulite size and optical properties. Other methods used to study crystallization behavior of such materials include differential scanning calorimetry (DSC) and x-ray diffraction (XRD).

8.3.1 Cross-polarized optical microscopy and atomic force microscopy

PEO crystallization

Cross-polarized optical microscopy (CPOM) was used to compare the crystal morphology between filled and unfilled PEO, and subsequently DSC studies were used to further quantify the relevant crystallization kinetics. We focus on systems with low silicate loadings ranging from neat PEO (0 wt.% MMT) to PEO with 10 wt.% MMT. In Fig. 8.4 we compare the CPOM images of neat PEO and a PEO/5 wt.% MMT intercalate, both crystallized at 45°C. The morphology of the crystals is shown at an early stage (neat: Fig. 8.4(a), intercalate: Fig. 8.4(c)) and at the final stage of crystallization (neat: Fig. 8.4(b), intercalate: Fig. 8.4(d)). For the neat PEO, it can be clearly seen that the spherulites are similar in size, and prior to impinging upon one another they appear circular, suggesting an isotropic (spherical) three dimensional shape. For the intercalated system (Figs 8.4(c)–(d)) the spherulite sizes vary a lot, and they are typically much smaller than the ones seen in neat PEO. Moreover, in these systems the spherulites are characterized by very anisotropic, non-spherulitic shapes (Fig. 8.4(d)) with jagged edges, even before impinging upon one another (Fig. 8.4(c)).

A CPOM time series, following a crystalline growth front in the same intercalated material, can provide some clues on the origin of these crystal morphologies. In Fig. 8.5 a progression of a growing crystallite is shown for the PEO/5 wt.% MMT system. The early and late stages are shown in Fig. 8.5(a) and Fig. 8.5(f), where silicate tactoids can be seen, manifested as either bright/white features (near the focused plane) or dark features (below and above the focused plane). Figs 8.5(b)–(e) are a higher magnification of the selected area (shown as the box in Figs 8.5(a)–(f)) as the spherulite growth-front encounters an MMT agglomerate (or a large tactoid). As the growth proceeds, the lamellar pathways are interrupted and they are forced to grow around the tactoid, breaking the spherical symmetry of the crystallite, and crystallization is delayed in the region downfield from the tactoid. The same behavior is also observed for the smaller tactoids in the image, albeit at smaller scale. At the end of crystallization (Fig.

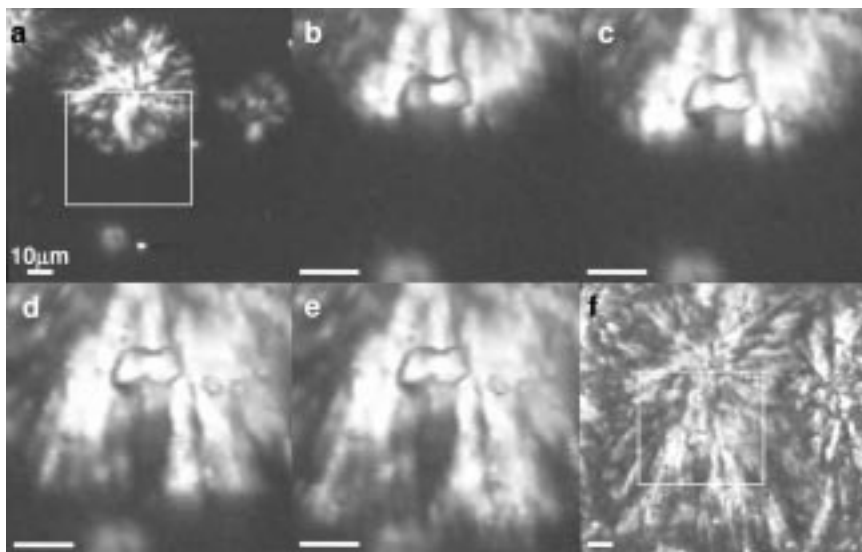


8.4 Cross-polarization optical microscope images of neat PEO (a,b) and PEO containing 5 wt.% MMT (c,d). Images on the left (a,c) are early in the crystallization process, while those on the right (b,d) are the final images. The scale bar is the same for all images (100 microns). White spots in (c) are tactoids found in the nanocomposite system. Image (d) illustrates the fact that later in the process many smaller spherulites grow to fill the space in the composite system. The growth front of the composite system (c) appears highly jagged in contrast with the very smooth front found in the neat PEO spherulites (a). Copyright © *Chem. Mater.* 2003, vol. 15, pp. 844–849.

8.5(f)) we see that the effect of the MMT on the crystallite growth, resulted in ‘spherulites’ grown in a haphazard fashion with tortuous lamellar pathways and jagged edges. Also, the crystallite size is markedly smaller than the spherulites developed in neat PEO (Fig. 8.4(b)).

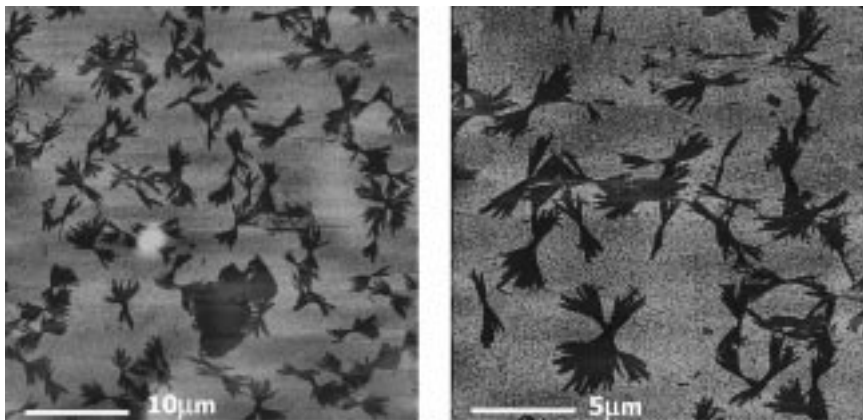
PVA crystallization

Before we consider the differences between neat and filled PVA systems, we shall briefly discuss how the crystallization of PVA develops in films cast from PVA/water solutions. As cast these films are mostly amorphous, and crystallites initiate predominately in the final drying stages; crystallization proceeds thereafter slowly, aided by the ambient humidity. If the ambient humidity is too low or absent the drying polymer becomes glassy and crystal growth becomes arrested before extended crystallites can develop and impinge. Though PVA has



8.5 A time series of cross polarization optical microscopy images of a nanocomposite region from PEO containing 5 wt.% MMT. Images (a) and (f) have the same magnification and are at the beginning (a) and the end (f) of the crystallization. The box in (a and f) outlines the area shown in (b–e) at a higher magnification, which focus on the growth of a spherulite ‘front’ as it encounters an MMT agglomerate. The scale bar in all images is 10 microns. Copyright © *Chem. Mater.* 2003, vol. 15, pp. 844–849.

a T_g above room temperature, water cast films still form crystals at ambient temperatures due to the slow drying nature of the hydrophilic polymer. Subsequently, plasticization by ambient humidity allows for a slow, cold crystallization of PVA resulting in crystals, which are reminiscent of structures as those from row nucleated crystallization in the earlier stages, dendritic in the mid to latter stages (Fig. 8.6), and spherulitic in final stages after they impinge and fully develop. The final systems include mature crystallites of all these morphologies, and this mixture of morphologies can only be described loosely as PVA dendrites or hedrites²⁵ due to the branched nature of the crystalline lamellae. These mature crystal structures are still not sufficiently birefringent to be observed with cross polarization microscopy. Before impinging on each other, the prevailing shape of the PVA crystallites on the surface of the film is a multi-directional ‘wheat sheaf’ structure as shown in Fig. 8.6. These crystallites are not spherically symmetric, i.e. they do not have a spherulitic symmetry, however, they do conjure up images of young or immature spherulites grown from the melt. The fact that these crystals are grown from water cast films has no bearing on the fundamental foci of this research; this preparation was only chosen as it allows for crystallization studies at room temperature and over extended time scales.

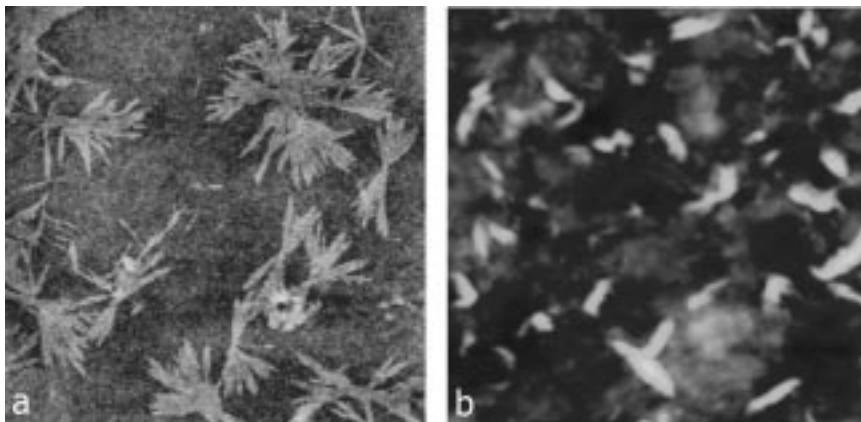


8.6 AFM images of bulk PVA ($40 \times 40 \mu\text{m}$, and $20 \times 20 \mu\text{m}$) obtained in contact mode (lateral force images shown). A variety of branched crystal morphologies –nearly impinging– are found throughout the film, however the same film is non-birefringent when viewed under a crossed polarized optical microscope. Copyright © *Macromolecules*, 2001, vol. 34, pp. 8475–8482.

PVA crystal morphology

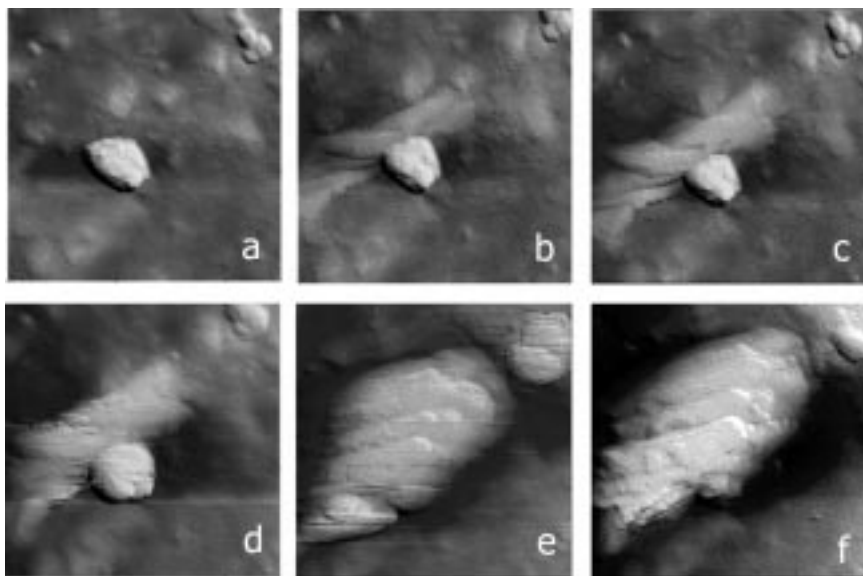
AFM was performed in all the above modes on bulk PVA films and on PVA filled with inorganic layers (4, 10, and 20 wt.% MMT) in order to measure differences in crystal morphology, with the emphasis on the initial stages of crystallization. As can be seen in Fig. 8.7(a), the bulk PVA has crystals which grow to sizes of about 5 microns and larger, before impinging upon neighboring crystallites and arresting further growth. In contrast, when inorganic filler layers are present (Fig. 8.7(b)) the crystallites are smaller and more linear in shape than the bulk crystallites. Crystallite sizes in the MMT-filled system are about 1–2 microns, when grown in the vicinity of the inorganic particles. The color scales used in both images, show the crystalline regions in lighter color, corresponding to higher apparent topography (i.e. smaller deformation under the constant applied force in addition to any true topography features). The behavior of PVA systems loaded with 10 and 20% MMT is similar to that of Fig. 8.7(b); i.e. crystals grow in a linear fashion, albeit in much higher density on the surface. Due to the higher crystallite densities the crystalline regions overlap, making it impossible to assign a diameter or length to these structures.

In order to elucidate the crystallization mechanisms responsible for this difference in morphology, we followed the evolution of the PVA crystals growing next to silicate layers or tactoids (the silicate particles imaged can be easily designated as layers or tactoids through their size: single layers are 1 nm thin, whereas tactoids – stacks of parallel packed single layers – are much larger, on the order of 100 nm). In Fig. 8.8, we follow the time evolution of PVA crystals in a $2.5 \times 2.5 \mu\text{m}$ region of a PVA/4 wt.% MMT sample, at room



8.7 Comparison between bulk PVA (a) and PVA/4 wt.% MMT (b), both $15 \times 15 \mu\text{m}$. Contact mode (height) images are shown under the high normal forces; the 'apparent topography' under these scanning conditions shows crystalline material in lighter colors, since it undergoes smaller compressive deformations. The modulus of the amorphous polymer in the PVA/MMT system (b) is much higher than the amorphous bulk (a), resulting in much smaller deformation under the same normal force, and thus in less contrast of the 'apparent topography'. There is a marked decrease in crystallite size and a change in shape when submicron inorganic particles are introduced in the PVA. Copyright © *Macromolecules*, 2001, vol. 34, pp. 8475–8482.

temperature and 50% relative humidity (due to its strong hydrophilicity, PVA tends to absorb water from the ambient humidity, resulting in plasticization as well as crystallization of PVA well below its known crystallization temperature of 193°C .) This image depicts well the general behavior found in the silicate filled system, i.e. the crystalline material found in Fig. 8.8 is indicative of the crystallites found in most images of the PVA/silicate systems studied here, as is evident in Fig. 8.7. Figure 8.8 shows a time series of height images, obtained by tapping AFM in the vicinity of a protuberant inorganic filler particle (a tactoid in this case). The crystalline PVA regions correspond to the apparent 'higher' features in Fig. 8.8; concurrent phase and force imaging show that these 'higher' features are much stiffer than the surrounding material, which is also confirmed by subsequent lateral force contact imaging. Thus we may safely conclude that the light-colored material is crystalline, and the darker-colored regions are amorphous. The PVA crystal initiates next to the inorganic surface (Fig. 8.8(a)), grows in size (Figs 8.8 (b)–(d)), and eventually covers completely the surface of the silicate (Fig. 8.8(e)). Furthermore, once the silicate becomes covered with PVA, it appears to continue to recruit amorphous polymer for crystallization in the same region (Fig. 8.8(f)), albeit slower than before. The tendency of the PVA to completely cover the tactoid in Fig. 8.8, which is typical also in all other regions of this sample, is driven by the strong specific interactions between the PVA and the silicate,¹⁶ which cause a strong wetting of the polymer on the



8.8 A time series of height images ($2.5 \times 2.5 \mu\text{m}$), obtained by tapping mode AFM in the vicinity of a protuberant inorganic filler tactoid. Time after casting is as follows: (a) 36 hours, (b) 3 days, (c) 4 days, (d) 6 days, (e) 20 days and (f) 21 days. The height scale (light to dark) is 400 nm (a–d) and 500 nm (e–f). The PVA crystal initiates next to the inorganic surface (a), grows in size (b–d), and eventually covers completely the surface of the silicate (e). The same crystallization behavior observed near the central protuberant tactoid, can also be seen for a smaller inorganic particle in the top right corner. Copyright © *Macromolecules*, 2001, vol. 34, pp. 8475–8482.

inorganic surface. The fact that these crystals grow in a linear fashion suggests that nucleation prefers to begin near the inorganic surface, and that once nucleated, the crystals tend to grow upon one another.

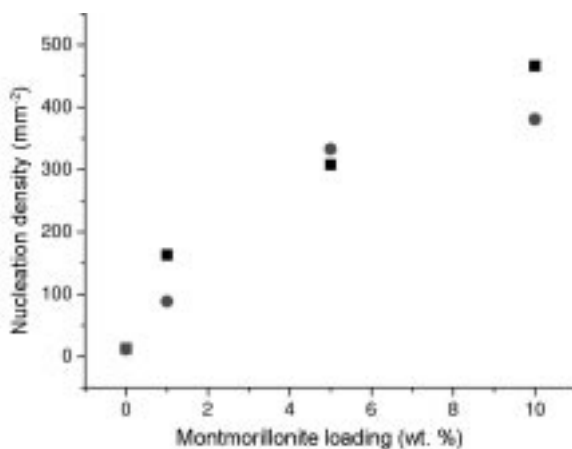
The PVA vinyl alcohol group forms hydrogen bonds with the silicate oxygens, which dominate the cleavage plane of MMT. Moreover, due to the atomically smooth MMT surface, these specific interactions are expected to force chains to create long adsorbed trains,²⁶ which in turn will promote a strongly interacting second layer of PVA to crystallize on top of them. Thus this MMT surface epitaxial/nucleating effect can be ‘felt’ through many layers of polymer, causing a long range collection and crystallization of PVA from the surface of the silicate (Fig. 8.8). Therefore, these sites tend to act as nucleating sites for the PVA crystallites. Accordingly scans of the PVA/4 wt.% MMT show many more crystallites per area compared to the neat PVA, as all the inorganic silicate fillers nucleate polymer crystallites. The PVA/MMT specific interactions decrease the surface energy necessary to create/nucleate a polymer crystal, and thus, the crystalline regions tend to nucleate around the silicate surfaces. Furthermore, since the silicate surface can be felt through only a small

distance, the new crystallites formed only grow to a limited size of about 2 microns. Hence, it is not unexpected that the size falls from 5 microns, in the neat PVA, to 1–2 microns in the MMT filled PVA (Fig. 8.7).

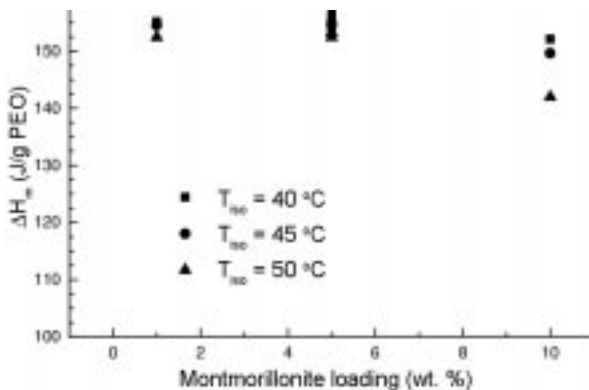
8.3.2 Differential scanning calorimetry and X-ray diffraction

PEO crystallite size

The difference in crystallite size for PEO crystallized in the presence of silicates can be quantified by enumerating the number of crystallites/spherulites per area. In Fig. 8.9 we show the density of crystallites, as measured in the isothermal crystallization CPOM experiments at temperatures (T_{iso}) of 45 and 50°C. It is seen that the density of crystallites increases by more than an order of magnitude when MMT layers are introduced in PEO, even at very small silicate loadings. Moreover, CPOM reveals that almost all of the crystal nuclei initiate in the bulk PEO, i.e. far away from the MMT fillers. Albeit this huge difference in the number of crystallites between neat and intercalated PEO, the polymer crystalline fraction – as measured through DSC experiments – does not show a marked change between these two systems. In Fig. 8.10 we plot the enthalpy of melting (ΔH_m) as measured by DSC, showing no strong effect of the silicate loading and/or the crystallization temperature on the final crystallinity of the systems. One of these DSC experiments is shown in Fig. 8.11(a) for neat PEO and PEO/5 wt.% MMT. The onset and peak crystallization temperatures (T_c) can also be measured from the cooling response (Fig. 8.11(b)). The addition of



8.9 The nucleation density as a function of silicate loading, as measured from cross polarization optical microscopy. Crystallization is done at 45°C (squares) and 50°C (triangles). The number of nucleated spherulites per unit area increases by more than tenfold, even at low silicate loadings. Copyright © *Chem. Mater.* 2003, vol. 15, pp. 844–849.

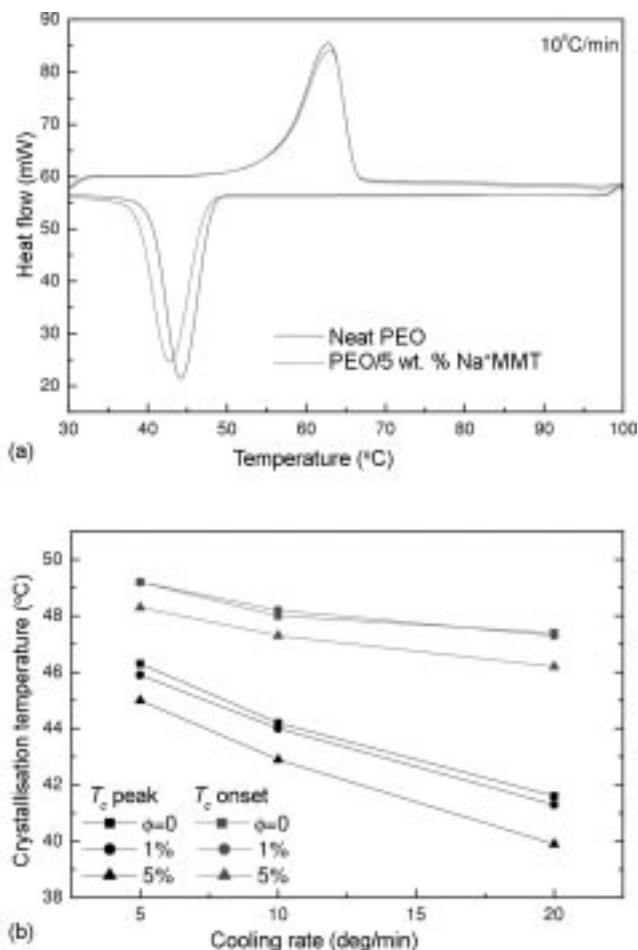


8.10 Enthalpy of melting for PEO versus filler loading. The PEO crystallinity does not change markedly with silicate loading, for various isothermal temperatures of crystallization ($T_{iso} = 40, 45,$ and 50°C : squares, circles, and up triangles, respectively). All samples were melted and then rapidly cooled to the T_{iso} ; after isothermal crystallization in the DSC, samples were heated at $10^{\circ}\text{C}/\text{min}$ and ΔH was measured. Copyright © *Chem. Mater.* 2003, vol. 15, pp. 844–849.

MMT fillers in the PEO decreases the polymer T_c for all cooling rates used, suggesting that the MMT hinders the PEO crystallization, a conclusion which is in concert with the behavior seen in Fig. 8.5. As expected, the DSC-observed T_c decreases with increasing cooling rate, and the crystallization temperature of PEO/MMT composite deviates more from the neat polymer's T_c as more MMT filler is added. The fact that the dependence of T_c on the cooling rate is similar for the neat PEO and the filled PEO suggests that these differences are due to genuine changes in the polymer crystallization, rather than changes of the thermal conductivity caused by the incorporation of the inorganic fillers. In the latter case, if the DSC-observed decrease of T_c were actually due to changes in thermal conductivity, the *difference in T_c* between the neat and filled PEO would have been a strong function of the cooling rate.

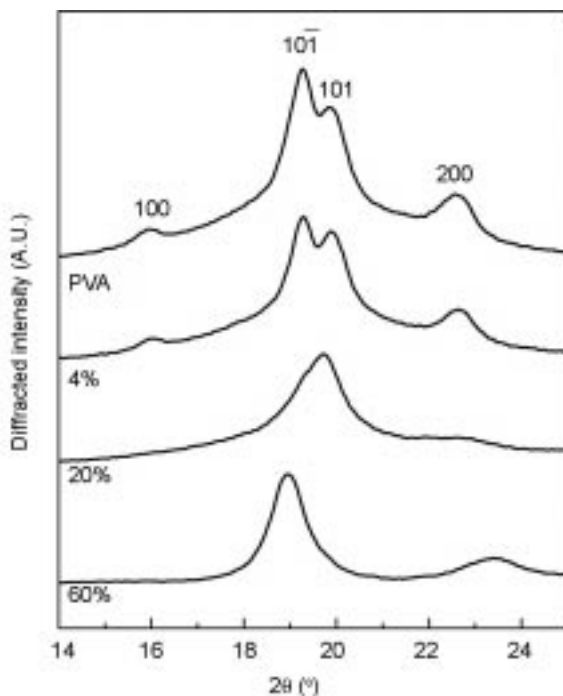
PVA crystal nature

In contrast to the PEO crystal behavior, the strong interactions present between PVA and the silicate surfaces bring about changes in the inherent crystal nature, as evidenced by the following observations. Wide angle XRD provides evidence that not only the crystal morphology but also the crystalline structure changes when the inorganic filler is added to PVA. Namely, in the 2θ region between 14.0 and 25.5° (Fig. 8.12) PVA has its 100, 101, 101 and 200 crystalline reflections (corresponding to $2\theta = 16.0, 19.4, 20.1$ and 22.7° respectively). The XRD scans in Fig. 8.12 (neat PVA and 4, 20, and 60 wt.% MMT) suggest that as silicate content increases from $\phi_{\text{MMT}} = 0$ to 20 wt.%, the 101 and $10\bar{1}$ peaks



8.11 (a) A typical DSC scan for PEO and PEO/5 wt.% MMT, at a heating/cooling rate of 10°C/min. (b) Peak and onset of the crystallization temperature, as a function of DSC cooling rate, for PEO and PEO/MMT nanocomposites. The crystallization temperature is decreasing with silicate loading, showing that a higher degree of undercooling is needed for crystallization of composites. Copyright © *Chem. Mater.* 2003, vol. 15, pp. 844–849.

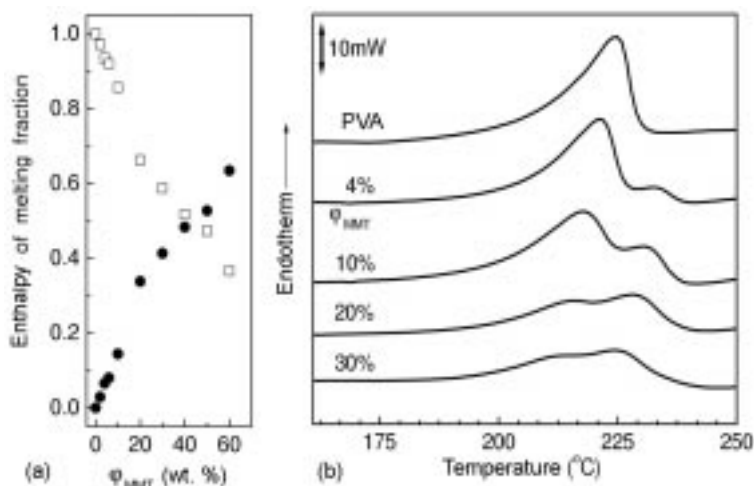
show a concerted decrease in intensity. This depression of the 101 and peaks is accompanied by the appearance of a single peak centered at $2\theta = 19.5^\circ$. This development of the diffraction peaks indicates that a new crystal structure forms with the addition of the silicate, at the expense of the bulk-like crystal structure. (For clarity, the XRD of the neat MMT is not given here. The appearance of the new peak, observed in the higher PVA loadings, is not connected in any way to crystalline reflections from the MMT structure.) Given the multiple overlapping peaks in the diffraction pattern, it is difficult to quantify with any accuracy



8.12 XRD curves of bulk PVA and silicate filled composites of various inorganic compositions. The bulk PVA reflections (100, 101, 101 $\bar{1}$ and 200) are at 2θ : 16.0, 19.4, 20.1 and 22.7°, respectively. With increasing inorganic content, there appears a concerted decrease in intensity of the 101 and 101 $\bar{1}$ peaks, accompanied by the appearance of a new peak centered at $2\theta = 19.5^\circ$, suggesting a new crystalline form for the clay-induced PVA crystals. Copyright © *Macromolecules*, 2001, vol. 34, pp. 8475–8482.

neither the difference of the crystallite sizes,²⁷ nor the simultaneous change in crystalline structure. However, the bulk-like and filler-induced crystals also have different melting temperatures (T_m) and DSC can be employed to quantify the change in crystalline structure with ϕ_{MMT} .

In Fig. 8.13(b), DSC traces are shown for the melting transitions of neat PVA films, as well as PVA films filled with MMT. Bulk PVA has a melting transition at $T_m = 225^\circ\text{C}$. As inorganic layers are added to PVA the polymer crystallinity does not change markedly, however a new, higher T_m crystalline form appears (Fig. 8.13(b)). Fig. 8.13(a) shows the inorganic content dependence of the fractions of the two melting transitions; these fractions are defined via the ratios of the corresponding enthalpies of melting over the total enthalpy of the sample, both for the bulk-like T_m , as well as for the new – higher T_m – melting transition observed in the presence of the inorganic fillers. Figure 8.13(a) clearly indicates that the presence of the inorganic surface induces a new higher T_m crystal at the



8.13 DSC traces showing the melting region of PVA/silicate composites of various chosen compositions. On the left, the fractions of the two melting enthalpies for the two crystalline forms for all the MMT concentrations studied [squares: bulk-like crystal ($T_m = 225^\circ\text{C}$), circles: higher T_m crystal]. The dependence of the enthalpy fractions on the ϕ_{MMT} suggests that the inorganic surface promotes a new, higher T_m crystal form, at the expense of the bulk crystalline material. Copyright © *Macromolecules*, 2001, vol. 34, pp. 8475–8482.

expense of the bulk-like crystals. This behavior is consistent with the XRD observation (Fig. 8.12) of a new crystal phase that gradually appears with the addition of the fillers, with a parallel depression of the bulk-like crystal peaks. Our AFM scans (Fig. 8.8) show that the inorganic-induced crystals grow around the inorganic fillers, and this suggests that the higher T_m may originate from the specific interactions near the PVA/silicate interface, which result in a strong polymer/inorganic adhesion.

8.4 Overview of nanocomposite structure and crystallization behavior

Using non-isothermal and isothermal DSC, and cross-polarization optical microscopy, we have investigated the differences of crystallization behavior in neat PEO films and PEO films filled by MMT inorganic layers. The coordination of PEO to the montmorillonite Na^+ promotes the polymer-filler miscibility, but renders the PEO/MMT interface not conducive to crystallization, since it promotes amorphous polymer conformations in the vicinity of the inorganic fillers. Thus, MMT causes a retardation of the crystal growth front, and results in crystal morphologies which are characterized by non-spherical shapes with jagged edges. Moreover, this PEO crystal obstruction by the MMT allows for the

'homogeneous' nucleation of large numbers of crystallites, which grow to much smaller sizes than neat PEO spherulites. In the Na^+ MMT filled PEO, crystallization nucleation sites occur in the bulk of the PEO matrix, i.e. far from the silicate surfaces, in considerably larger numbers than in unfilled PEO at the same undercooling. This higher nucleation density is a manifestation of two effects: (a) the disruption of the spatial continuity by the inorganic layers, which allows for the independent nucleation of PEO crystallites in the spaces between the fillers, and (b) the characteristic PEO/ Na^+ coordination, which markedly inhibits 'heterogeneous' nucleation by the MMT fillers. The absence of marked heterogeneous nucleation contrasts the PEO behavior against most of the other polymer/MMT systems studied, where heterogeneous nucleation and/or epitaxial crystallization are the dominant effects. Despite the different crystal morphologies between neat and filled PEO, there is no marked change in polymer crystal fraction for the small amounts of silicate ($\phi_{\text{MMT}} < 10\%$) studied here. For larger MMT loadings than studied here, the introduction of more PEO/MMT interfaces in the system decreases the PEO crystallinity proportionally to ϕ_{MMT} .^{28,29}

Using AFM, we have investigated the differences in neat PVA films and PVA films filled by MMT inorganic layers. Mechanical variations across polymer surfaces – as those between amorphous and crystalline regions – are manifested in various AFM imaging modes, including contact, intermittent contact, and two force modes. Since in most cases the mechanical variations are superimposed on surface topographical features, sometimes comparative imaging with various modes is needed to unambiguously resolve polymer crystal, amorphous polymer, and filler particles.

When inorganic layers (MMT) are added to the PVA polymer, crystallites are initiated and grown in the immediate vicinity of the inorganic surface. We believe that this is due to the strong specific interactions between the inorganic surfaces and the polymer. The crystallites found near the inorganic fillers are about 2 microns in size, smaller than the crystallites found in the neat PVA film, which are 5 microns or larger. Moreover, the melting temperature of these crystals was found to be higher than the bulk T_m . At the same time, XRD also shows differences in the PVA crystalline structure when crystallized in the presence of MMT, suggesting that the inorganic fillers change also the crystal structure. This new, silicate-induced PVA crystal phase is promoted by the existence of the montmorillonite layers, and forms at the expense of the bulk PVA crystalline phase.

8.5 Materials properties of poly(vinyl alcohol)/ Na^+ montmorillonite nanocomposites

The purpose of this study is, first, to investigate the structure of the PVA/MMT nanocomposites, with the focus on the layered filler dispersion, as well as on the changes of the polymer crystallinity due to the inorganic layered fillers.

Subsequently, through the study of selected nanocomposite material properties, we attempt to correlate the hybrid structure with changes in the material response. The structure is explored over the full range of silicate compositions. On the other hand, properties are explored only for the low silicate loadings, which are relevant to potential applications.

8.5.1 Thermal properties

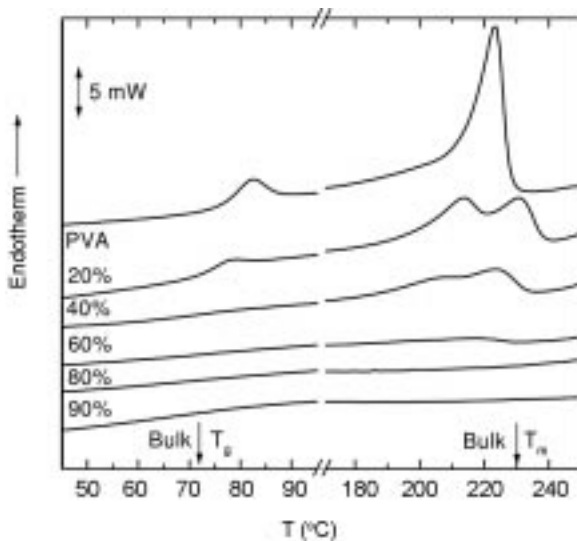
The model water soluble polymer/silicate nanocomposite systems presented here also possess unique thermal properties which can be studied using various techniques. These include DSC and thermal gravimetric analysis. Thermal properties for the PVA/silicate system are outlined in the following sections.

DSC and XRD analysis of PVA crystallites in the nanocomposite

Thermal characterization

Bulk PVA has a glass transition at $T_g = 70^\circ\text{C}$ and a melting transition at $T_m = 225^\circ\text{C}$. For fully intercalated PVA hybrids (i.e. all the polymer is intercalated in MMT galleries) DSC does not detect any traces of thermal transitions between 35°C and 250°C (Fig. 8.14), hybrids with $\phi_{\text{MMT}} > 60$ wt.%). For these 'neatly intercalated' nanocomposites, both the T_g and T_m are either too weak and/or too broad to measure, or they are suppressed due to the polymer confinement. Although the physical origins of this behavior are still under debate,^{30,31} this absence of thermal events is in agreement with the general behavior of polymers intercalated in clays and synthetic silicates. In a plethora of systems studied: nylon-6,² PEO,^{9,10} PMPS,³⁰ PS,³¹ PCL,³² PMMA³³ intercalated in naturally occurring silicates (MMT) and in synthetic layered aluminosilicates (fluorohectorite), there exist no detectable thermal transitions for the intercalated polymers, over a wide temperature range below the T_g and above the T_m . Despite the use of methods with an increasing resolution and sensitivity (such as DSC, thermally stimulated current, positron annihilation, NMR, and so on) no transitions can be detected in neatly intercalated systems. For example, TSC, DSC, and NMR studies^{9,10} of an intercalated poly(ethylene oxide) (PEO, $M_w = 100,000$)/MMT hybrid (20 wt.% polymer), indicated the absence of any thermal transitions between -100°C and 120°C , that could correspond to the vitrification or the melting of PEO ($T_g = -55^\circ\text{C}$ and $T_m = 65^\circ\text{C}$). On a local scale, intercalated polymers exhibit simultaneously fast and slow modes of segmental relaxations for a wide range of temperatures,^{10,30,31} but again with a marked suppression (or even absence) of cooperative dynamics typically associated with the glass transition.

A systematic study of the DSC traces with ϕ_{MMT} (Fig. 8.14) shows that the T_g and T_m signals weaken gradually, and disappear for ϕ_{MMT} above 60 wt.%. This

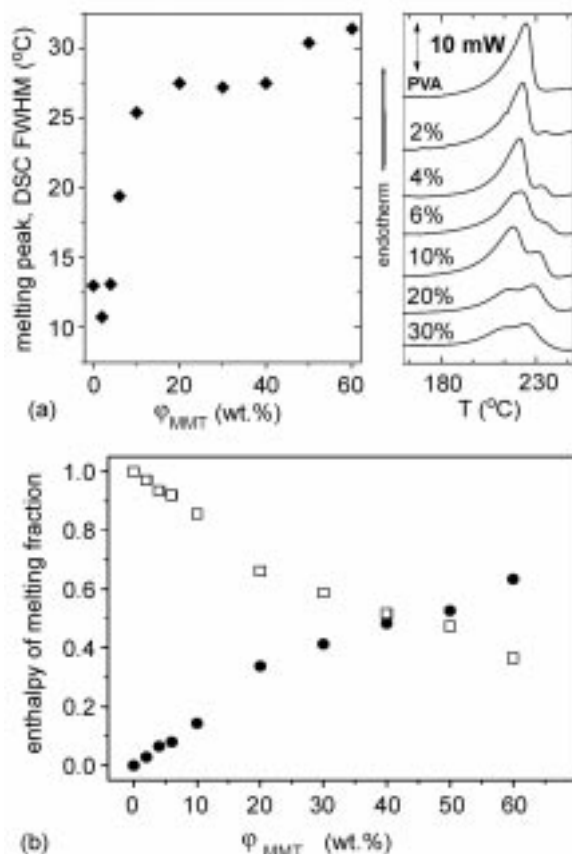


8.14 Differential scanning calorimetry of PVA/MMT nanocomposites with varying ϕ_{MMT} (20°C/min, second heating). For clarity a featureless region is omitted between 95 and 175°C. Copyright © *Chem. Mater.* 2000, vol. 12, pp. 2943–2949.

suggests that in these systems ($\phi_{\text{MMT}} > 60$ wt.%) all the polymer is affected by the inorganic layers, and there seems to be no bulk-like PVA present (at least not enough to manifest itself through thermal transitions). For higher polymer concentrations (e.g. 20 wt.% MMT) there appear two distinct and overlapping melting peaks, one around the bulk T_m and another one at higher melting temperature.

PVA crystallinity

The PVA melting was studied by performing DSC on several high PVA concentration nanocomposites ($2 < \phi_{\text{MMT}} < 30$ wt.%, Fig. 8.15(a)). Compared to the neat PVA, in the nanocomposites appears also a new higher- T_m crystal phase. This dual DSC melting trace is reminiscent of DSC endotherms belonging to a PVA system studied by Tanigami *et al.*³⁴ In their system, Tanigami *et al.* controlled the PVA stereoregularity by using blends of a syndiotactic-rich and an atactic poly(vinyl alcohol). What was observed was a crystalline-phase-separated system which exhibited a dual melting point. That dual melting point arose from two crystal phases: one formed primarily by syndiotactic sequences, the other primarily by atactic sequences. The two types of crystals have melting points which differ by about 15–22°C (T_m at 228 and 250°C). This T_m difference is comparable to the one measured for our PVA/MMT nanocomposites, as shown in Fig. 8.15. The width at half-maximum (FWHM), for the combined



8.15 DSC of the melting region for the low MMT content nanocomposites ($20^\circ\text{C}/\text{min}$); (a) FWHM of the combined melting endotherms and corresponding DSC traces around T_m ; (b) the fractional heat of fusion owing to the MMT-induced crystal phase (circles, $T_m = 235^\circ\text{C}$) and bulk-like crystal phase (squares, $T_m = 225^\circ\text{C}$), as determined from the DSC peak fittings. Copyright © *Chem. Mater.* 2000, vol. 12, pp. 2943–2949.

DSC melting peak, was used as an indicator of how the two crystal phases were present in the PVA blend. To calculate FWHM, the peak value of the DSC trace is located. The full width of the melting peak is then evaluated at a distance halfway between the peak value and the DSC trace baseline. In Tanigami's work, the melting peak FWHM increased to $25\text{--}35^\circ\text{C}$ when the atactic-rich and the syndiotactic-rich phases coexisted, whereas it remained approximately 10°C when either of the two crystal phases was in excess. The FWHM for our nanocomposite combined/dual melting peaks is plotted in Fig. 8.15(a), as a function of the silicate loading (ϕ_{MMT}). The full width increases sharply from about 13°C to above 25°C as the silicate composition crosses the percolation

threshold ($\phi_{\text{MMT}} = 4$ wt.%). This suggests that we have substantial volumes of bulk-like and of MMT-induced crystal phases coexisting for $\phi_{\text{MMT}} > 5$ wt.%.

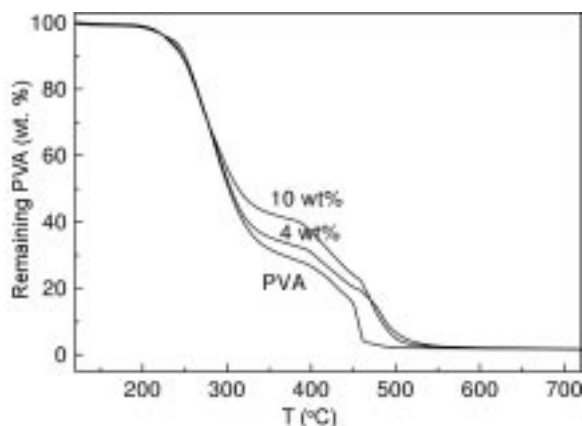
In order to quantify the relative volumes of the two crystal phases present, we used the standard fitting method³⁵ and gaussian functions to estimate the melting enthalpies (heat of fusion, ΔH) for each of the two melting peaks in the DSC trace. The fraction of the two melting enthalpies (Fig. 8.15(b)) will reflect the relative amount of the respective crystalline phases in the polymer matrix. The new crystal form – which appears when MMT fillers are added to the PVA – seems to grow linearly with the MMT concentration, and at the expense of the bulk-like PVA crystal phase (Fig. 8.15(b)). This clearly suggests the high T_m phase is induced by the presence of the silicate layers. The shape of the melting peak and the relative peak areas remain the same in subsequent DSC scans, after cooling from the melt state (exotherms not shown). This indicates that this dual crystalline melting, is not an artifact of the solution casting or the thermal history, but is indeed induced by the presence of the silicate.

Wide angle XRD provides evidence that we actually have a new crystal phase in the nanocomposite. Namely, in the 2θ region between 14.0 and 25.5° (Fig. 8.12) PVA has its 100, $10\bar{1}$, 101 and 200 crystalline reflections (corresponding to $2\theta = 16.0, 19.4, 20.1$ and 22.7° , respectively). In the same region MMT also has its 101 reflection at 19.7° . We have annealed our samples at 245°C for 35 minutes prior to scanning in order to allow for higher quality PVA crystals. Samples showed some degradation by becoming brown in color and overall crystallinity did decrease somewhat; however, the DSC of the annealed samples remains the same qualitatively (dual melting peak) and quantitatively (heat of fusion). The XRD scans in Fig. 8.12 suggest that as silicate content increases from $\phi_{\text{MMT}} = 0$ to 20 wt.%, the 101 and $10\bar{1}$ peaks concurrently become lower in intensity and are replaced by what appears to be a single peak centered at $2\theta = 19.5^\circ$. This is consistent with the DSC measured high- T_m crystal phase that appears at these compositions, and with its gradual enhancement at the expense of the bulk-like crystal. Unfortunately, a quantitative comparison between the DSC and the XRD is not possible, as the existence of 5 overlapping diffracted reflections does not allow for the unambiguous fitting of the XRD peaks.

In summary, the analysis of the PVA crystalline XRD and DSC data shows that at low silicate loadings (below 60 wt.%) there appears a new crystalline phase, which is induced by the presence of MMT. This phase grows linearly with ϕ_{MMT} at the expense of the bulk PVA crystal phase. For $\phi_{\text{MMT}} \geq 60$ wt.%, PVA is primarily intercalated and no melting endotherms are found for the confined polymer.

Thermal degradation

In addition to having a higher melting point, thermal degradation properties of PVA/MMT nanocomposites also show improvement. A comparative thermal



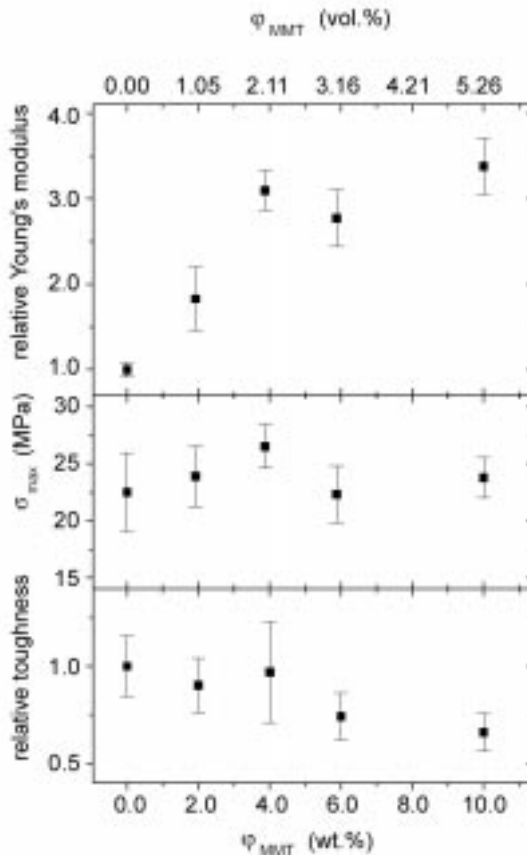
8.16 Polymer weight loss from TGA scans in air, for PVA and two nanocomposites containing 4 wt.% and 10 wt.% Na⁺ MMT. Copyright © *Chem. Mater.* 2000, vol. 12, pp. 2943–2949.

gravimetric analysis (TGA) of pure PVA and two nanocomposites with 4 and 10 wt.% MMT (10°C/min in air) is shown in Fig. 8.16. The weight loss due to the decomposition of PVA is nearly the same until the temperature of about 275°C. After this point, the silicate inhibits the PVA weight loss, which reaches a maximum lag of about 75°C. Unlike most other polymer/MMT nanocomposite systems,³³ this PVA/MMT suffers nearly the same weight loss as the bulk for its initial 50%, possibly due to the fact that PVA can supply oxygen from within to initiate its decomposition.

8.5.2 Mechanical properties

Exfoliated polymer/silicate systems have been found to exhibit mechanical, thermal and solubility properties, as well as water vapor transmission rates, which are superior to conventionally filled systems.²⁶ Furthermore due to their nanoscale dispersion of filler, they retain optical clarity.³⁶ In our PVA/MMT hybrids, and especially at the application relevant low ϕ_{MMT} (below 10 wt.%), TEM and XRD reveal a coexistence of intercalated and exfoliated silicate layers. For these systems we will briefly describe some of their materials properties.

Tensile tests were performed on PVA nanocomposite films with silicate loadings of 0, 2, 4, 6 and 10 wt.%. Because completely dry PVA films are quite brittle, tests were performed at a nominal relative humidity of 50%, according to the usual testing procedure for PVA.³⁷ Prior to testing, films were equilibrated in a humidity chamber at 90% r.h. Yielding was not found for any of the samples. All samples had an initial period of elastic deformation followed by a nearly monotonically increasing stress during plastic deformation, until failure. Figure 8.17 shows the Young's modulus, the stress-at-break and strain-at-break, and the



8.17 Tensile testing results as a function of MMT weight and volume content. Top: the Young's modulus normalized by the bulk value (68.5 MPa); middle: the maximum stress at break; bottom: the toughness of the hybrids normalized by the bulk values (45.8 kJ/m²). Copyright © *Chem. Mater.* 2000, vol. 12, pp. 2943–2949.

measured fracture toughness, all as a function of silicate loading. For comparison, the Young's moduli are normalized by the measured bulk PVA value (68.5 MPa). At $\phi_{\text{MMT}} = 4 \text{ wt.}\%$, the nanocomposite is characterized by a modulus about 300% larger than the one of the respective bulk PVA. In most conventionally filled polymer systems, the modulus increases linearly with the filler volume fraction; for these nano particles much lower filler concentrations increase the modulus sharply and to a much larger extent.¹ Accordingly, in the PVA/MMT systems the dependence of modulus on ϕ_{MMT} is very strong at very low content, and tends to level off after $\phi_{\text{MMT}} = 4 \text{ wt.}\%$, at about 3.5 to 4 times the value for bulk PVA. This behavior has been reported before for poly-(dimethyl siloxane)/MMT exfoliated hybrids.^{38,39} The dramatic enhancement of

the Young's modulus for such extremely low MMT filler concentrations can not be attributed simply to the introduction of the higher modulus inorganic filler layers. A recent theoretical approach is assuming a layer of affected polymer on the filler surface, with a much higher Young's modulus than the bulk equivalent polymer. This affected polymer can be thought of as the region of the polymer matrix which is physisorbed on the silicate surfaces, and is thus stiffened through its affinity for and adhesion to the filler surfaces.³⁸ Obviously, for such high aspect ratio fillers as our MMT layers, the surface area exposed to polymer is huge (for MMT is typically 700–800 m²/g), and the dramatic increases in the modulus with very low ϕ_{MMT} are not surprising. Furthermore, beyond the percolation limit ($\phi_{\text{MMT}} > 4 \text{ wt.}\%$) the additional exfoliated layers are introduced in polymer regions that are already affected by other MMT layers, and thus it is expected that the enhancement of Young's modulus will be much less dramatic.

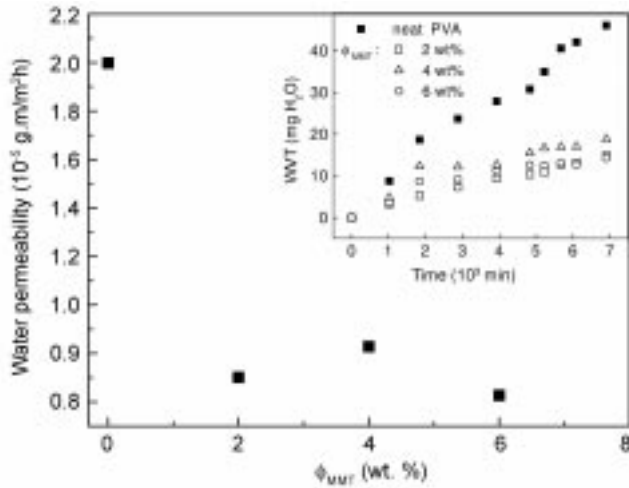
The stress at break (σ_{max}) is also plotted versus the silicate content in Fig. 8.17. The data shows that σ_{max} is relatively insensitive to the filler concentration. Finally, the toughness is also plotted in the same graph, again normalized by the bulk PVA value (45.8 kJ/m²) for comparison; the toughness was calculated from the integrated area under the Instron stress/strain curve. There is a very moderate decrease of the toughness (3% at $\phi_{\text{MMT}} = 4 \text{ wt.}\%$, and 22% at $\phi_{\text{MMT}} = 6 \text{ wt.}\%$) for ϕ_{MMT} , which is caused by a comparable decrease of the strain-at-break.

8.5.3 Barrier properties

With the dispersion of these ultra-thin inorganic layers throughout the polymer matrix, the barrier properties of the nanocomposites are expected to be strongly enhanced compared to the respective polymer. The water vapor transmission rates were measured for the pure polymer and several of its low ϕ_{MMT} nanocomposites, and are plotted in Fig. 8.18. In the same figure, the resulting water permeabilities⁴⁰ are plotted as well. WVT and permeabilities were measured following ASTM E96, for PVA and PVA/MMT nanocomposite films of the same thickness ($8.98 \pm 0.33 \times 10^{-3} \text{ cm}$). The permeabilities decrease to about 40% of the pure WVT values for silicate loadings of only 4–6 wt.%. We believe that this enhancement in the water permeability originates both from the increased path tortuosity of the penetrant molecules – forced around the inorganic layers – as well as the enhanced modulus of the polymer matrix in the nanocomposites.

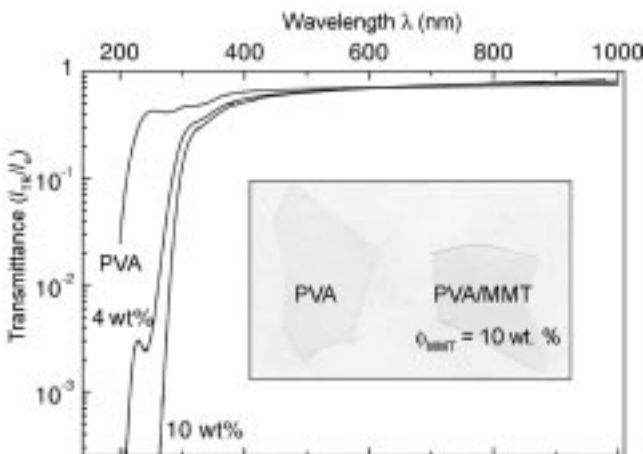
8.5.4 Optical properties

Because of the nanoscale dispersion of the silicates in the PVA matrix, optical clarity remains high at silicate contents which yield primarily exfoliated composites. This allows its potential use in paper coatings, one of the most



8.18 Water vapor permeability for the neat PVA and several PVA/MMT nanocomposites. The inset shows the water vapor transmission raw data collected for each composition, which were used to calculate the water permeabilities. Copyright © *Chem. Mater.* 2000, vol. 12, pp. 2943–2949.

common uses for pure PVA. Figure 8.19 shows the UV/VIS transmission spectra of pure PVA, and PVA/MMT hybrids with 4 and 10 wt.% MMT. These films have thicknesses of 0.17, 0.18 and 0.15 mm, respectively. The spectra show that the visible region (400–700 nm) is not affected at all by the presence of the silicate, and retains the high transparency of the PVA. For the ultraviolet wavelengths, there is strong scattering and/or absorption, resulting in very low



8.19 UV-VIS transmittance spectra of PVA and PVA/MMT nanocomposites containing 4 and 10 wt.% MMT. Copyright © *Macromolecules*, 2001, vol. 34, pp. 8475–8482.

transmission of the UV light. This is not surprising as the typical MMT lateral sizes are 50–1000 nm.

8.6 Conclusions

We have investigated the structure and properties of PVA/MMT nanocomposites formed by water casting, a solution intercalation method. From TEM and XRD studies, over the full range of silicate loadings, we find that there is a coexistence of exfoliated and intercalated silicate layers. The system becomes mostly intercalated as silicate loading increases beyond $\phi_{\text{MMT}} \geq 60$ wt.%. The exfoliation of layers is attributed to the water casting method used, since the water suspended layers become kinetically trapped by the polymer and can not reaggregate. DSC studies find a suppression of the thermal transitions (T_g and T_m) for the purely intercalated systems. However, for the mostly exfoliated, low MMT loading nanocomposites, DSC unveils a new melting transition with higher T_m than the neat PVA. X-ray diffraction of the polymer crystals suggest that this is a new, silicate-induced PVA crystal phase, that is promoted by the existence of the montmorillonite layers at the expense of the bulk-like PVA crystalline phase.

Some basic materials characterization was also performed for the low ($\phi_{\text{MMT}} \leq 10$ wt.%) MMT loadings. For these MMT concentrations the inorganic layers are well dispersed throughout the PVA matrix, i.e. the nanocomposites formed are mostly exfoliated hybrids. The mechanical/tensile properties of these nanocomposites were studied for low silicate loadings and Young's modulus was found to increase by 300% for 5 wt.% silicate, with only a 20% decrease in toughness, and no sacrifice of the stress at break compared to the neat PVA. In addition, for these low loadings, thermal stability from TGA measurements was shown to be slightly enhanced, and high optical clarity was retained. Additional properties at low silicate loadings, detailed studies of the PVA crystal morphology, and NMR investigations of the PVA segmental dynamics in intercalated structures, are currently under way.

8.7 References

1. Giannelis, E.P.; Krishnamoorti, R.K.; Manias, E. *Adv. Polym. Sci.* **1998**, *138*, 107.
2. Kojima, Y.; Usuki, A.; Kawasumi, M.; Okada, A.; Kurauchi, T.T.; Kamigaito, O. *J. Polym. Sci., Part A: Polym. Chem.* **1993**, *31*, 983. (b) Kojima, Y.; *et al. J. Polym. Sci., Part B: Polym. Phys.* 1995, *33*, 1039.
3. Lan, T.; Kaviratna, P.D.; Pinnavaia, T.J. *Chem. Mater.* **1995**, *7*, 2144. (b) Wang, M.S.; Pinnavaia, T.J. *Chem. Mater.* **1994**, *6*, 468. (c) Pinnavaia, T.J. *Science* **1983**, *220*, 365.
4. Kanatzidis, M.G.; Wu, C.G.; Marcy, H.O.; DeGroot, D.C.; Kannewurf, C.R. *Chem. Mater.* **1990**, *2*, 222. (b) *Chem. Mater.* **1991**, *3*, 992. (c) *Chem. Mater.* **1996**, *8*, 525.
5. Vaia, R.A.; Ishii, H.; Giannelis, E.P. *Chem. Mater.* **1993**, *5*, 1694. (b) Vaia, R.A.;

- Jandt, K.D.; Kramer, E.J.; Giannelis, E.P. *Macromolecules* **1995**, *28*, 8080. (c) Vaia, R.A.; Price, G.; Ruth, P.N.; Nguyen, H.T.; Lichtenhan, J. *Appl. Clay Sci.* **1999**, *15*, 67.
6. Krishnamoorti, R.K.; Vaia, R.A.; Giannelis, E.P. *Chem. Mater.* **1996**, *8*, 1728. (b) Giannelis, E.P. *Adv. Mater.* **1996**, *8*, 29.
 7. Gilman, J.W.; Jackson, C.L.; Morgan, A.B.; Harris, R.; Manias, E.; Giannelis, E.P.; Wuthenow, M.; Hilton, D.; Philips, S.H. *Chem. Mater.* **2000**, *12*, 1866.
 8. Carrado, K.A.; Thiyagarajan, P.; Elder, D.L. *Clays and Clay Minerals* **1996**, *44*, 506.
 9. Vaia, R.A.; Vasudevan, S.; Krawiec, W.; Scanlon, L.G.; Giannelis, E.P. *Adv. Mater.* **1995**, *7*, 154. (b) Vaia, R.A.; Sauer, B.B.; Tse, O.K.; Giannelis, E.P. *J. Polym. Sci., Part B: Polym. Phys.* **1997**, *35*, 59.
 10. Wong, S.; Vaia, R.A.; Giannelis, E.P.; Zax, D.B. *Solid State Ionics* **1996**, *86*, 547.
 11. Bassner, S.L.; Klingenberg, E.H. *Am. Ceram. Soc. Bull.* **June 1998**, 71.
 12. Bassett, D.C. *Principles of Polymer Morphology*; Cambridge University Press: Cambridge, 1981. (b) Lee, J.-C.; Nakajima, K.; Ikehara, T.; Nishi, T. *J. Appl. Polym. Sci.* **1997**, *64*, 797. (c) Mi, Y.; Chen, X.; Guo, Q. *J. Appl. Polym. Sci.* **1997**, *64*, 1267. (d) Wang, C.; Chen, C.-C. *Polym. Bull.* **1999**, *43*, 433. (e) Mucha, M.; Marszalek, J.; Fidrych, A. *Polymer* **2000**, *41*, 4137. (f) Stocker, W.; Schumacher, M.; Graff, S.; Thierry, A.; Wittmann, J.-C.; Lotz, B. *Macromolecules* **1998**, *31*, 807. (g) Doye, J.P.K.; Frenkel, D. *J. Chem. Phys.* **1998**, *109*, 10033.
 13. Janigova, I.; Chodak, I. *Eur. Polym. J.* **1995**, *31*, 271. (b) Liang, J.Z.; Li, R.K.Y.; Tjong, S.C. *J. Appl. Polym. Sci.* **1999**, *71*, 687. (c) Tjong, S.C.; Xu, S.A. *Polym. Int.* **1997**, *44*, 95. (d) Alonso, M.; Velasco, J.I.; de Saja, J.A. *Eur. Polym. J.* **1997**, *33*, 255. (e) Radhakrishnan, S.; Saujanya, C. *J. Mater. Sci.* **1997**, *64*, 1267. (f) Stricker, F.; Bruch, M.; Mulhaupt, R. *Polymer* **1997**, *38*, 5347. (g) Trifonova, D.; Varga, J.; Vancso, G.J. *Polym. Mater. Sci. Eng.* **1998**, *41*, 341.
 14. Davis, R.D.; Jarrett, W.L.; Mathias, L.J. *Polym. Mater. Sci. Eng.* **2000**, *82*, 272.
 15. Liu, L.; Qi, Z.; Zhu, X. *J. Appl. Polym. Sci.* **1999**, *71*, 1133.
 16. Strawhecker, K.; Manias, E. *Chem. Mater.* **2000**, *12*, 2943.
 17. Strawhecker, K.; Manias, E. *Macromolecules* **2001**, *34*, 8475.
 18. Manias, E.; Touny, A.; Wu, L.; Strawhecker, K.; Lu, B.; Chung, T.C. *Chem. Mater.* **2001**, *13*, 3516.
 19. Lincoln, D.M.; Vaia, R.A.; Wang, Z.-G.; Hsiao, B.S.; Krishnamoorti, R. *Polymer* **2001**, *42*, 9975.
 20. Vaia, R.A.; Giannelis, E.P. *Macromolecules* **1997**, *30*, 7990.
 21. Balazs, A.C.; Singh, C.; Zhulina, E. *Macromolecules* **1998**, *31*, 8370.
 22. Wu, J.; Lerner, M. *Chem. Mater.* **1993**, *5*, 835.
 23. Hackett, E.; Manias, E.; Giannelis, E.P. *Chem. Mater.* **2000**, *12*, 2161.
 24. Kuppa, V.; Manias, E. *Chem. Mater.* **2002**, *14*, 2171.
 25. Bassett, D.C. *Principles of Polymer Morphology*; Cambridge University Press: Cambridge, 1981.
 26. Israelachvili, J. *Intermolecular and Surface Forces*; Academic Press: London, 1991.
 27. Guinier, A. *X-ray Diffraction in Crystals, Imperfect Crystals, and Amorphous Bodies*; W.H. Freeman: San Francisco, 1963.
 28. Menakanit, S. M.Sc. Thesis, Penn State University, 2002.
 29. Strawhecker, K. PhD. Thesis, Penn State University, 2002.
 30. Anastasiadis, S.H.; Karatasos, K.; Vlachos, G.; Giannelis, E.P.; Manias, E. *Phys. Rev. Lett.* **2000**, *84*, 915.

31. Zax, D.B.; Yang, D.K.; Santos, R.A.; Hegemann, H.; Giannelis, E.P.; Manias, E. *J. Chem. Phys.* **2000**, *112*, 2945.
32. Messersmith, P.B.; Giannelis, E.P. *Chem. Mater.* **1993**, *5*, 1064.
33. Bandiopadhyay, S.; Giannelis, E.P. *Polym. Mater. Sci. Eng.* **2000**, *82*, 2008.
34. Tanigami, T.; Hanatani, H.; Yamaura, K.; Matsuzawa, S. *Eur. Polym. J.* **1999**, *35*, 1165.
35. Perkin-Elmer DSC7 Manual, 1994.
36. Wang, Z.; Pinnavaia, T.J. *Polym. Mater. Sci. Eng.* **2000**, *82*, 278.
37. Sundararajan, P.R. In *Polymer Data Handbook*; Mark, J.E., Ed.; Oxford University Press: New York, 1999; p. 894.
38. Shia, D.; Hui, C.Y.; Burnside, S.D.; Giannelis, E.P. *Polym. Compos.* **1998**, *19*, 608.
39. Burnside, S.D.; Giannelis, E.P. *Chem. Mater.* **1995**, *7*, 1597.
40. ASTM Standard E 96-95, Standard Test Methods for Water Vapor Transmission of Materials, Annual Book of ASTM Standards, April 1999, p 829.